

NASA Technical Memorandum 83556

(NASA-TM-83556) ICE SHAPES AND THE
RESULTING DRAG INCREASE FOR A NACA 0012
AIRFOIL (NASA) 31 F HC A03/MF A01 CSCL D1C

N85-27839

Unclass
G3/03 21532

Ice Shapes and the Resulting Drag Increase for a NACA 0012 Airfoil

William Olsen, Robert Shaw,
and James Newton
*Lewis Research Center
Cleveland, Ohio*

Prepared for the
Twenty-second Aerospace Sciences Meeting
sponsored by the American Institute of Aeronautics and Astronautics
Reno, Nevada, January 9-12, 1984

NASA



ICE SHAPES AND THE RESULTING DRAG INCREASE FOR A NACA 0012 AIRFOIL

William Olsen, Robert Shaw, and James Newton

National Aeronautics and Space Administration
Lewis Research Center
Cleveland, Ohio 44135

SUMMARY

Experimental measurements of the ice shapes and resulting drag increase were measured in the NASA Icing Research Tunnel. The measurements were made over a large range of conditions (e.g., airspeed and temperature, the drop size and liquid water content of the cloud, and the angle of attack of the airfoil).

Additional results are given which are helpful in understanding the ice structure and the way it forms, and in improving the ice accretion modeling theories. There are data on the ice surface roughness, on the effect of the ice shape on the local droplet catch, and on the relative importance of various parts of the ice shape on the drag increase. Experimental repeatability is also discussed.

INTRODUCTION

Part of the NASA icing research program involves the development of analyses to predict the ice accretion on airfoils and the resulting aerodynamic penalty. Extensive experimental data for ice accretion and the resulting drag are being obtained for several representative airfoils to add to the existing data base. The emphasis is on airfoils of current interest. The airfoil covered in detail in this paper is the NACA 0012 airfoil.

Detailed measurements were made of the ice accretion and the resulting drag in the NASA Lewis Icing Research Tunnel (IRT). These data were obtained over a range of air temperature, airspeed airfoil angle of attack, spray time, liquid water content and drop size. The results can be used in the development of computer codes to predict the ice accretion and resulting drag. The drag results are compared to the existing correlation (ref. 1). Additional experiments were performed to improve our understanding of icing, such as: the ice structure, surface roughness, the effect of ice shape on the droplet catch, and what part of the ice shape is important.

APPARATUS AND PROCEDURE

The NACA 0012 airfoil model, the Icing Research Tunnel (IRT), and the instrumentation used to measure the drag coefficient are discussed in this section.

Description of the IRT

The IRT is a closed loop low speed refrigerated wind tunnel. Its test section (fig. 1), is 1.83 m high and 2.74 m wide. The airspeed in the test

section can be varied from 30 to 480 km/hr, and the total temperature can be varied from above 0 °C down to about -30 °C. According to the present calibration, the icing cloud issuing from 77 air atomizing nozzles can produce a drop size range of from below 10 to about 40 microns (volume median diameter, DVM). The liquid water content (LWC) in the test section can be varied from about 0.3 to 3.0 g/m³. Not all combinations of DVM and LWC are possible at every airspeed. The DVM and LWC are set according to the present calibration by adjusting the air and water pressures to the spray nozzles. (The symbols used are defined in appendix A.) For details about the spray cloud calibration and a discussion of possible error sources, refer to reference 2. The results in reference 2 indicate that the data reported herein should be free of any significant error.

Airfoil Model

The airfoil model used in this test program is a 0.53 m chord NACA 0012 airfoil. This model was mounted on the turntable in the IRT as shown in figures 1 and 2. This arrangement permitted simple changes of the airfoil angle-of-attack. The airfoil used was a portion of a UH1H helicopter main rotor blade. Like all rotor blades, this airfoil section had a small twist (one-half degree per foot of span), therefore the angle-of-attack of the airfoil was set at the center of the tunnel where the ice shape and section drag would be measured. As will be shown in the Results, the effects of using a production helicopter airfoil are negligible.

Drag Measurements

The section drag at the center-span of the airfoil model was measured with a standard traversing wake survey probe. The pitot-static probe is shown positioned, downstream of the airfoil model in figure 1. The probe was two airfoil chords downstream of the airfoil.

Drag wake surveys were taken only after the IRT spray cloud was turned off and the air was cloud free. While the spray system was on, the probe was retracted behind an anti-iced shield to prevent ice accretion on the small unheated tip of the pitot-static probe. The probe support was anti-iced.

When activated, the wake survey probe automatically traversed the wake behind the wing. The speed of the traversing probe was adjusted before the test program so that no lags in the probe response existed. For further details and a discussion of possible errors refer to appendix B, where it was concluded that there were no significant errors.

Test Matrix and Procedure

The test matrix is listed in table I. The ice shape and resulting drag coefficient depend upon at least the following: the airfoil shape and angle of attack, the air temperature and velocity, and the LWC and DVM of the cloud. With that number of parameters, only a sparse matrix of conditions and repeat conditions could be accomplished.

The test procedure followed for most of the data runs is listed below:

- (1) The model angle-of-attack (α) was set.
- (2) The desired IRT airspeed (V) and total air temperature (T) are set.
- (3) The wind tunnel spray system was adjusted to the desired drop size (DVM) and liquid water content (LWC). If the spray time was to be short then the cloud settings were pre-set, so that data were not affected by the time to adjust the cloud.
- (4) After the desired spray time had elapsed, the icing spray system was turned off.
- (5) The tunnel was brought down to idle and the frost aft of the ice accretion was removed with a scraper. Tufts on the airfoil were also deiced.
- (6) The wake survey probe was then traversed across the airfoil wake with the tunnel at the desired airspeed.
- (7) The tunnel was again brought to idle and the following were performed at the centerspan of the airfoil: (a) a narrow slit was cut in the ice down to the airfoil surface and the airfoil ice shape was traced on a piece of cardboard that was precut to fit the shape; (b) a template with a ruled grid was slipped into the ice slot and the ice was photographed from the same position relative to the airfoil; (c) the airfoil was then heated to obtain ice samples, which were placed in a freezer for later photographs of the ice structure and plaster casts of the ice sample.
- (8) The airfoil was then totally cleaned free of ice and the next test was performed.

RESULTS AND DISCUSSION

This section primarily contains information about the effect of the icing parameters on the ice shape and resulting drag. The icing parameters are spray time, angle of attack, airspeed, total temperature, drop size and liquid water content. There are data related to the quality of the experiment. In addition, there are other results which will be useful for the development of an improved ice accretion theory.

Quality of the Data

Most questions about the quality of the tunnel flow, the icing cloud and its calibration, and the drag measurements are discussed in reference 2 and appendix B. Reported in this section are data quality tests that are specific to this airfoil test and where an important conclusion is reached.

Comparison to published dry airfoil drag results. - Figure 3 shows how the drag coefficient for the dry airfoil varied with angle of attack. Much of this dry airfoil data came from the first run of every night of icing tests; this was used as a quality control reference for the drag data. Plotted on this figure is the published curve fit of data measured in aerodynamic wind

tunnels for smooth 0012 airfoils (ref. 3). A band is shown to account for the Reynold's number range of the dry airfoil data ($2 \times 10^6 < Re < 3.2 \times 10^6$). This good agreement suggests that concerns about using a section of a production helicopter rotor blade are unfounded. The wake survey probe measurements are also qualified by this good agreement.

Repeatability of the dry airfoil drag measurements. - Twenty seven repeat measurements of the drag coefficient, C_D , were made with the dry 0012 airfoil at a 4° angle of attack during the course of the experimental program. The average value of the drag coefficient was 0.00814. The percent variation¹ of that data was 7.7 percent of the average value. That kind of scatter is typical of wind tunnel data.

Repeatability of the ice shapes and drag. - Figure 4(a) shows the repeatability of the ice shape and resulting drag coefficient for a typical rime ice shape accreted at -26°C . The ice shapes and resulting drag coefficients repeat quite well; the scatter in the drag coefficient is comparable to the scatter observed with the dry airfoil data. Figure 4(b) is a similar rime ice repeatability comparison for a different icing condition. The rime ice shape and drag coefficient repeated well again. The percent variations for both sets of C_D data is about ± 5 percent, which is close to the percent variation noted for the clean airfoil data.

Similar comparisons are made in figures 5(a) and (b) for two glaze ice shapes. There is a much larger variation in the ice shapes and drag coefficient for one case on each figure. The percent variations for both sets of C_D data is about ± 15 percent of the average values of C_D . This is much larger than the percent variation noted for the rime shapes or for the clean airfoil. Poor repeats have also been noted in other airfoil tests with glaze ice. No certain explanation for the poor repeatability of glaze ice shapes is available at this time.

Effect of Angle of Attack

Figure 6(a) shows how the section drag coefficient varies with angle of attack for one ice shape; a typical rime ice shape that was accreted at a 4° angle of attack. The drag measured at several angles for the clean airfoil is also plotted in figure 6(a). The drag is at least 50 percent higher than the drag for the clean airfoil.

Figure 6(b) contains a similar drag-angle sweep, except that the ice is a severe glaze ice shape. This glaze ice shape increased the drag coefficient considerably; about four times larger than the clean airfoil drag coefficient. Above an angle of about 6° , the flow over the entire upper (suction) surface separated, as evidenced by tufts along the surface of the airfoil. Therefore, subsequent icing tests in this program were generally limited to less accretion time and to smaller angles in order to avoid bad separation with glaze ice.

$$^1 \text{Percent variation} = \left(\frac{\text{Standard deviation of } C_D \text{ data}}{\text{Average value of } C_D} \right) \times 100$$

In figures 7(a) and (b) the ice accretion at different angles of attack is shown. The effect of angle of attack upon the ice shape and the resulting drag is shown on figure 7(a) for an icing condition that produces rime ice. Figure 7(b) is similar but the icing condition produced glaze ice. In this case only weak separation occurred at the 8° angle. The clean airfoil drag-angle data are also plotted in figures 7(a) and (b) for comparison.

Effect of Accretion Time

The effect of the accretion time on the ice shape is shown on figure 8. The ice was accreted at several angles; each for two icing conditions. Cases A, B, and C share the same icing condition, which produces glaze ice. Each case is at a different angle of attack and involves as many as three sprays at different accretion times (2, 5, and 15 min). Cases D, E, and F are similar, except that the icing condition for these 3 cases produces a rime type of ice. Please note that all accretion times reported herein should be corrected (reduced by 1/4 min) to account for the time it takes the cloud to attain a steady value.

The ice shapes clearly show the ice accretion history (i.e., growth rings) starting from the initial dry airfoil out to a 15 min growth. Notice that the horns in cases A and B are starting to show in the 5 min ice shape, but not in the 2 min shape.

The drag data for these cases are not reported here. These data were taken early in the program before it was realized that the frost buildup on the aft surfaces of the airfoil must be removed in order to achieve accurate drag measurements that are representative of flight. In natural icing flights there is no frost buildup. Appendix b describes the results of an experiment to determine the effect of frost on the drag measurement.

Effect of Temperature

Temperature has the greatest effect upon the ice shape and the ice structure. The photographs on figure 9 show the ice, on both sides of the airfoil, at one temperature. Figure 10(a) shows how the ice shape changes with increased temperature for two icing conditions. The ice shape tracing at 209 km/hr and a total temperature of -15 °C corresponds to the photographs in figure 9. The ice at the coldest temperature (-26 °C) is white and pointed at the stagnation point, which is typical of rime ice. As the temperature increases the shape gradually changes to a horn shaped glaze ice. When the total temperature is very close to 0 °C the impinging droplets run off and do not freeze. The two icing conditions on figure 10(a) were done at the same DVM and the same upstream droplet mass ($LWC \cdot V \cdot \tau = \text{constant}$), with the 0012 airfoil at a 4° angle of attack.

The variation of the section drag coefficient with temperature for each icing condition is plotted on figure 10(b). The drag coefficient variation with total temperature is similar for each condition. The peak drag coefficient occurs at about -5 °C, which corresponds to where the horns are the largest. Below about -15 °C the drag coefficient does not change much, because the ice shape does not change much.

Ice Structure

The structure of the ice is very dependent upon the temperature at which it forms. A good way to look at the ice structure is to cut off thin ice samples (about 0.3 cm thick) from the ice accreted on the airfoil and then photograph them with backlighting. The samples shown on figure 11 were obtained during the experiment at 209 km/hr: the results of which are shown on figure 10. Rime ice is opaque and therefore appears to be black when backlit in figure 11, rather than white as it appears under normal lighting.

Some unique features of the ice structure are apparent in the backlit photos in figure 11. For example, there are very large bubbles in the ice formed at high temperatures (-2 and -8 °C). There are curious streaks in the ice accreted at -15 and -18 °C. Upon close inspection of the actual ice these streaks are thin filaments that are either voids or perhaps rime ice. At the upper and lower edges of the four coldest ice shapes, closely packed rime ice feathers (look black when backlit) have formed. The individual spread-out rime feathers that are downstream on the lower surface are lost during the ice sampling process.

Additional information about the ice structure can be obtained by looking at very thin ice samples under polarized light. Individual ice crystals can be seen because each crystal will polarize the light differently and produce a different color. Figure 12 shows the polarized light results in black and white for glaze and rime ice samples. The conditions for these samples are essentially the same as two cases on figure 11: the streaked glaze ice at -15 °C and the rime ice at -26 °C. These photos show that the ice crystals for the streaked glaze condition are very large, whereas the rime ice crystals are very small. The large crystals are normally formed by a gradual freezing process, whereas the small crystals for rime ice suggests the freezing process was rapid. Do not be confused by the superimposed grid lines showing through the rime ice sample.

Effect of Airspeed

Airspeed can have a large effect on the ice shape and the resulting section drag coefficient, as evidenced by the results on figure 13. Only the velocity was varied in this comparison. This data set and the data set at 209 km/hr on figure 10(b) form part of a three dimensional plot showing the combined effects of airspeed and temperature. The very large horns accreted at the highest airspeed were so large they caused the flow to separate over the entire suction side of the airfoil.

Effect of Drop Size

The effect of droplet size is shown on figures 14(a) and (b) for a number of cases (A to F). The icing conditions for each case are different; they are listed in the table on figure 14(a). Each case involves a large variation in the drop size (DVM) with each other parameter held constant. Figure 14(b) shows the effect of drop size on the ice shape, while figure 14(a) shows the effect upon the resulting drag coefficient. Cases A and E are glaze ice cases that exhibit a very large drop size effect upon the ice shape and resulting drag. In particular, the drop size has a very large effect on the angular location of the upper surface horn. The effect on the other glaze ice shapes

(B and D) is much less. Rime ice case C shows little change in the shape; only the effect of the larger catch efficiency with bigger drops is shown. In case F the ice changed from rime to more like glaze. Cases A, B, C, and F share the same icing conditions with the 209 km/hr data set on figure 10. By using these two data sets, one could plot a three dimensional plot showing the combined effects of drop size and total temperature. It shows that the drop size effect is greatest wherever the temperature effect is greatest.

Effect of LWC

Figure 15 shows the effect of liquid water content (LWC) on the ice shape and the resulting drag coefficient for two icing conditions where only LWC was varied. Except for the highest LWC for the -18°C case, the ice shape changed very little in shape. These two data sets also form a three dimensional plot with figure 10 which shows the combined effects of LWC and total temperature. Once again, the LWC effect is greatest wherever the temperature effect is greatest.

Roughness of the Ice Surface

The roughness of the surface of the ice was sampled for a few of the cases previously described. A small strip of ordinary modeling clay was pressed on to the ice to make a mold of the ice surface. The clay impression was then photographed.

The effect of temperature on the roughness in the stagnation region is shown by a series of photographs on figure 16(a). The roughness of the ice surface is obviously a strong function of temperature. The size of the roughness elements, (i.e. the height of the hills) varies from about 0.2 cm at -8°C down to less than 0.01 cm at the lowest temperatures.

The effect of time on the ice roughness is shown by the photographs on figure 16(b). These photos show that for the glaze ice conditions the roughness increases with time, rapidly at first then at much slower later. Rime ice, not shown here, never gets rough compared to glaze.

Although no other clay molding was done, a close look at the photographs of the ice accretion for each run reveals additional information about roughness changes for glaze ice. Increased drop size increases the size of the roughness up to a point, then the roughness decreased with increased drop size. Airspeed seems to have a small effect; but that would not be true when kinetic heating becomes important at higher airspeeds.

Effect of Ice Shape and Roughness on Droplet Catch

Old ice accretion theory ignores the effect of ice shape on the local droplet catch.

To test this thesis, a simple and direct technique was used to determine how the ice shape and its roughness affects the local droplet catch. It used the fact that droplets freeze on impact under rime icing conditions. A 3 min rime spray was accreted on top of an initial ice shape. The airspeed and DVM

are the same as for the initial ice, because these variables affect the catch. After the 3 min spray, a thin sample of the two-layer ice was removed from the airfoil, backlighted, and photographed. Two initial ice shapes were used: one was a 15 min glaze ice shape and the other was a 15 min rime ice shape. Figure 18 gives a measure of the local droplet catch on the initial glaze and rime ice shapes by simply measuring the local variation of the thickness of 3 min rime spray on top. The initial rime ice was sprayed with water soluble dye to differentiate the initial rime ice from the additional rime ice.

A few things stand out from these photos. The additional rime spray only accreted on the upstream surfaces of the initial rime and glaze ice shapes. The accretion for the rime shape is greatest on the spike. The maximum accretion for the glaze shape occurred on the horns and also on top of the local roughness hills. There was no accretion in the cavity for the glaze ice on figure 18; which could explain the large voids in the ice. There is no accretion on the sides, only on the upstream surfaces. These results suggest that the local catch effect of the ice shape and roughness can explain the differences between rime and glaze ice shapes when only the temperature is changed.

Effect of Partial Ice Removal

Gray (ref. 1) suggested that the ice on the upper surface near the leading edge makes the predominant contribution to the drag of an airfoil. That would mean that an ice accretion theory or a deicing system could concentrate on treating the upper surface ice. Let us put this thesis to the test at an icing condition favoring the thesis; namely a glaze ice shape with large horns. The ice shape used in this test is shown on figure 19; the ice was accreted at 4° then the drag was measured at several angles of attack (i.e., a drag-angle sweep). Ice was then removed below cut A and another drag-angle sweep was made. A similar drag-angle sweep was made after ice above cut B was removed from a repeated ice accretion. These three drag-angle sweeps were plotted on figure 19. Clearly the bottom horn of ice (pressure side) is generally less important than the suction side horn; but it cannot be neglected even for this case, which favored Gray's thesis.

Comparison With Old Correlation

Gray (ref. 1) correlated the change in the section drag coefficient to the icing time, airspeed, LWC, total and maximum catch efficiencies, total temperature, and the airfoil geometry. The airfoil geometry includes the chord length, leading edge radius/chord, the angle of attack and the angle of attack at which ice was accreted. The change in section drag coefficient, ΔC_D , is the drag coefficient for the iced airfoil minus the clean airfoil drag coefficient.

Gray's correlation was formulated from limited data for six types of airfoils over a wide range of icing conditions. The predictions from Gray's correlation for the 0012 airfoil test conditions are compared to the measured values of ΔC_D on figure 20. The line of perfect agreement gives a reference to determine how well the predicted values of ΔC_D agree with the measured values of ΔC_D . Only a few points fall near the line of perfect agreement. Gray's correlation overpredicts the change in drag by a substantial amount. The same poor agreement was noted in reference 4 with a large

G/A wing in the IRT. We cannot offer an explanation for this bad agreement at this time.

CONCLUDING REMARKS

1. Extensive data for ice shapes and the resulting drag were obtained for a NACA 0012 airfoil over a wide range of icing conditions. These data will be useful in evaluating and formulating ice accretion analyses and also performance penalty predictions.

2. The old correlation by Gray for the drag increase caused by ice agreed poorly with the measured results. This same poor agreement has been noted by other recent investigators.

3. Additional results were obtained which will prove helpful in understanding and predicting the ice accretion: ice structure, roughness, effect of ice shape on droplet catch, and what parts of the ice shape are important.

APPENDIX A
NOMENCLATURE

C	airfoil chord, m
C_D	section drag coefficient of the airfoil
C_{Dclean}	drag coefficient of clean airfoil
C_{Diced}	drag coefficient of iced airfoil
ΔC_D	$C_{Diced} - C_{Dclean}$
DVM	volume median drop size; μm
LWC	liquid water content, g/m^3
P_{tw}	total pressure in the wake, N/m^2
P_w	static pressure in the wake, N/m^2
$P_{t\infty}$	total pressure in free stream, N/m^2
P_∞	static pressure in free stream, N/m^2
y	transverse coordinate across wake, m
Re	Reynold's number for the airfoil
τ	time, min
T	total temperature, $^\circ\text{C}$
V	airspeed, km/hr

APPENDIX B
DRAG MEASUREMENTS

This appendix discusses the wake survey method used to measure the drag coefficient, how it was calculated, the transducers used, and some possible error sources.

Description of wake survey. - The section drag of the 2D wing model in the center-span plane (see traverse path on fig. 1(b)) was measured using a conventional traversing wake survey probe. The probe is two airfoil chords downstream of the airfoil trailing edge as shown in figure 1(a).

When activated, the wake survey probe automatically traversed the wake of the airfoil. The traverse speed of the probe was adjusted so that no lags in the probe response existed. Drag surveys were only taken when the IRT cloud was turned off and the air was free of any cloud. While the spray was on the probe was positioned behind an anti-iced protective shield to prevent ice from being accreted on its tip. The probe was not heated in order to keep the probe tip as small as possible. The probe support was anti-iced.

Calculation of the section drag coefficient. - As the probe traversed the wake, the instantaneous analog signals from the four pressure transducers as well as a signal from a position potentiometer were digitized by an A/D converter. The digital information was passed on to the NASA Lewis central data recording/computing facility where that data was converted to engineering units. The wing section drag coefficient was calculated using the Jones equation (ref. 5):

$$C_D = \frac{2}{C} \int_{\text{wake}} \sqrt{\frac{P_{tw} - P_w}{P_{t\infty} - P_\infty}} \left\{ 1 - \sqrt{\frac{P_{tw} - P_w + (P_w - P_\infty)}{P_{t\infty} - P_\infty}} \right\} dy \quad (C1)$$

In order to determine the appropriate end points to be used in the drag coefficient integral, an on-line plot was displayed during the test program for each data reading which showed the difference in total pressure ($P_{t\infty} - P_{tw}$) as a function of probe position. From this plot, the viscous wake end points could be identified and the drag coefficient could then be calculated.

The effects of the blockage caused by the wake survey traverse were accounted for in this calculation. Tunnel velocity measurements with and without the airfoil in place indicated that the blockage caused by the traverse increased the local incident airspeed by approximately 4 percent. The tunnel blockage caused by this very small airfoil can be neglected.

Transducers. - A 15 psi absolute transducer was used to measure the local total pressure level sensed by the probe. A 1 psi differential pressure transducer was used to measure the total-minus-static pressure level sensed by the pitot-static probe tip. A similar pressure transducer was used to measure the IRT airspeed well upstream of the airfoil. All four transducers are located outside of the test section to shield them from the extreme temperature environment inside of the test section.

Effect of cloud nonuniformity on drag measurements. - The LWC of the icing cloud in the IRT is not uniform across the entire span of the airfoil (1.8 m). The uniform region is over the middle .6 meters of the tunnel; the LWC then drops to near zero at the tunnel walls. Therefore the ice shape in the middle third of the span will be uniform, but the upper and lower thirds of the span will have less ice. Will this nonuniform ice accretion affect the drag coefficient measured at the center span of the airfoil? The easiest way to check to see if it does is to gradually remove the ice from the top and bottom of the airfoil span and observe how the measured drag changes. Figure 21 contains the drag results of two experiments where the ice span was gradually reduced from the full tunnel span down to only the middle 0.3 meters. For the glaze and rime ice shapes this major reduction in the span of ice had only a small effect on the measured drag. Clearly a large uniform cloud is not necessary for adequate section drag measurements in the center of the span. This conclusion should also be true for less severe ice shapes and for lower angles of attack.

Effect of frost. - One of the problems with testing in an icing facility with its turbulent saturated airstream, is that a very thin frost layer will collect on the aft parts of the airfoil. Frost does not normally occur in flight. The IRT turbulence intensity is low (about one-half percent) but flight turbulence would be an order of magnitude lower. The higher turbulence is believed to be the cause of the unnatural frost build up in the IRT on the aft surfaces. Does this aft frost have to be removed before accurate drag measurements can be made?

A simple experimental comparison is made on figure 22 using the same glaze and rime icing conditions that were used in figure 21. The drag is measured as sprayed without removing the thin frost layer over the aft surfaces of the airfoil. Then the aft frost layer is scraped off down to the bare airfoil surface. Figure 22 shows that the thin frost layer can have a large effect on the measured drag coefficient when the drag rise of the ice is small, such as with rime ice. The effect of the frost is not so great with glaze ice. To be on the safe side all aerodynamic measurements were made with the frost removed.

The rime feathers on the lower surface (see the photographs on fig. 9) were then removed to see what affect they would have at one angle. Figure 23 shows that their affect is small compared to the effect of the ice shape and the frost. Rime feathers are also seen in flight tests into natural icing.

REFERENCES

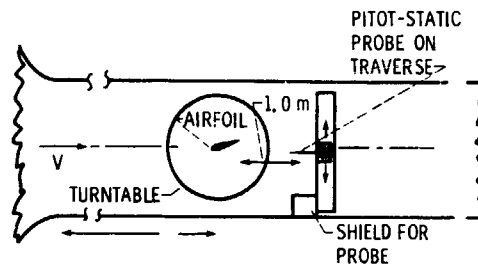
1. Gray, V.H., "Prediction of Aerodynamic Penalties Caused by Ice Formations on Various Airfoils," NASA TN D-2166, 1964.
2. Olsen, W., Takeuchi, D., and Adams, K., "Experimental Comparison of Icing Cloud Instruments," AIAA Paper 83-0026, 1983.
3. Abbott, I.H., and Von Doenhoff, A.E., Theory of Wing Sections Including a Summary of Airfoil Data, Dover. New York, 1958.
4. Shaw, R.J., Sotos, R.G., and Salano, .R., "An Experimental Study of Airfoil Icing Characteristics," AIAA 82-0283, 1982.
5. Gregorek, G., Hoffmann, M.J., Weislogel, G.S., and Vogel, G.M., "In-flight Measurements of the GAW-2 Aerodynamic Characteristics," SAE Paper 770461; Mar. 1977.

GENERAL REPORT
OF POOR QUALITY

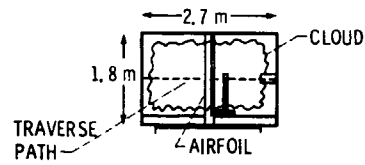
TABLE I. - TEST CONDITIONS FOR ICING TESTS WITH NACA 0012 AIRFOIL, 0.53 m CHORD

Run number	Tunnel conditions		Spray conditions			Angle of attack, deg		Drag coefficient, C _D	Comment											
	Airspeed, km/hr	Total temperature, C	LWC, g/m ³	DVM, μm	Time, min	Spray	Aero													
Varying time and angle																				
SH-1	209	-8	2.1	20	5	0	0	Drag not reported because frost was not removed in these early runs												
SH-2					15	0	0													
SH-3					2	0	0													
SH-4					15	4	4													
SH-5					5	4	4													
SH-6					2	4	4													
SH-7					15	8	8													
SH-8					5															
SH-9					2															
SH-10					15															
SH-11					2															
SH-12					15	4	4													
SH-13					5	4	4													
SH-14					2	4	4													
SH-15					15	0	0													
SH-16					5	0	0													
SH-17					2	0	0													
Drag angle sweep with one ice shape																				
0-10	209	-8	2.1	20	5	4	4	0.02767	Bad flow separation α > 5.5°											
0-11							8	.02647												
0-12							2	.02421												
0-13							0	.02199												
0-14							-3	.02683												
0-15							5.5°	.0358												
0-26							4	0.01077												
0-27							8	.01610												
0-28							11	.03148												
0-29							-3	.01268												
0-30							0	.01172												
Ice shape and drag variation with angle																				
0-4							209	-8		2.1	20	5	4	4	0.03382	Some flow separation for run 0-9				
0-8													0	0						
0-9													8	8						
0-26													4	4						
0-31													0	0						
0-32	8	8																		
Effect of temperature																				
S-29	209	-2	1.3	20	8	4			4				0.02807							
S-30		-1											.02647							
S-31		-5											.06036							
S-32		-8											.02949							
S-44													.021							
S-70		-18											.02161, .0210							
S-45		-26											.0194							
S-69		-15											.02105							
S-36		-12											.02072							
S-72		-20											.01773							
S-113		-2					1.05	20		6.2	4	4	0.0756							
S-114		-8											.0606							
S-115		-12											.0370							
S-116		-17											.0284							
S-117		-26											.0238							
Effect of velocity																				
S-33	149	-8	1.3	20	8	4	4	0.01622	Bad flow separation for run S-35											
S-34	209							.0296												
S-35	338							.1182												
Effect of drop size																				
S-22	209	-8	1.3	26	8	4	4	0.07493												
S-23				20				.03884												
S-24				14				.01465												
S-88				36				.10455												
S-25				338				-8		1.05	26	5.2	4	4	0.1266					
S-26											20				.0951					
S-27				209				-26		1.3	14	8	4	4	.0309					
S-53											26				0.0196					
S-57											20				.0190					
S-58											14				.01206					
S-50											-8				1.3	20	3	4	4	0.01941
S-81																				26
S-52				-26				1.3		26	8	4	4	.01154						
S-53														0.0196						
S-57														.0193						
S-58														.0121						
S-59				-2				1.3		26	8	4	4	0.0344						
S-60	0.02905																			
S-61	.03147																			
Effect of LWC																				
S-94		-8	1.0	20	8	4	4	0.0262												
S-95		1.3	.0307																	
S-96		1.6	.0456																	
S-109		-18	1.0					20		8	4	4	.0212							
S-110		1.3	.0246																	
S-111		2.0	.0312																	

ORIGINAL PAGE IS
OF POOR QUALITY



(a) Top view of test section.



(b) Test section - looking downstream.

Figure 1. - Location of airfoil and wake survey traversing probe in the test section of the IRT.



Figure 2. - The 0012 Airfoil and the Wake Survey Probe in the IRT.

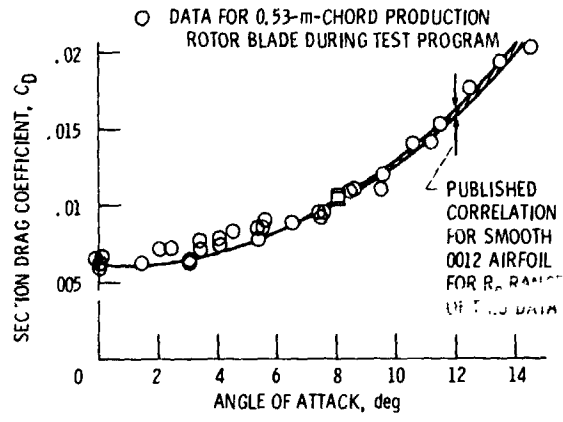
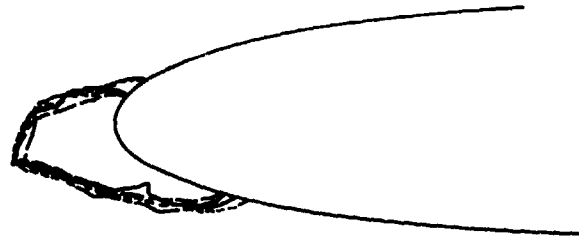


Figure 3. - Comparison of measured clean airfoil data with published data for the 0012 airfoil.

C_D	DIFFERENCE FROM AVERAGE C_D , PERCENT
0.01941	0.9
.02009	4.5
.01812	-6.0
.01930	.4

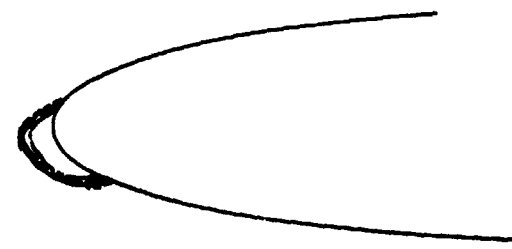
% VARIATION, \pm 4.0 PERCENT



(a) DVM, 20 μ m; LWC, 1.3 g/m^3 ; time, 8 min.

.01053	3.0
.01077	5.3
.01003	-2.0
.00957	-6.4

% VARIATION, \pm 5.0 PERCENT

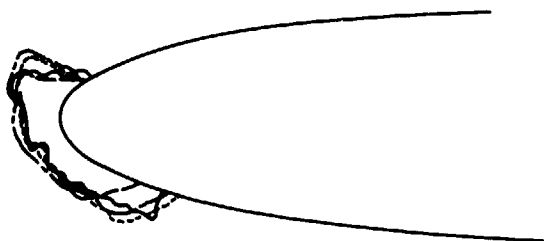


(b) DVM, 12 μ m; LWC, 1.08 g/m^3 ; time, 5 min.

Figure 4. - Repeatability of ice shape and drag for rime ice shapes. Total temperature, $-26^{\circ}C$; airspeed, 209 km/hr; 0.53-m-chord 0012 airfoil at 4° .

C_D	DIFFERENCE FROM AVERAGE
0.03382	-3.4
.02767	-21.0
.03729	+6.5
.04134	+18.0

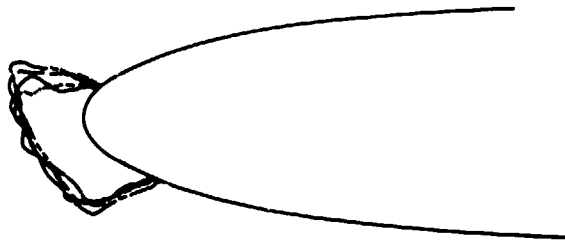
% VARIATION, ± 16.0 PERCENT



(a) DVM, 20 μm ; LWC, 2.1 g/m^3 ; time, 5 min.

.02960	-8.0
.03074	-4.4
.02949	-8.3
.03884	+20.7

% VARIATION, ± 14.0 PERCENT



(b) DVM, 20 μm ; LWC, 1.3 g/m^3 ; time, 8 min.

Figure 5. - Repeatability of ice shape and drag for glaze ice shapes. Total temperature, -8°C ; airspeed, 209 km/hr ; 0.53-m-chord 0012 airfoil at 4° angle.

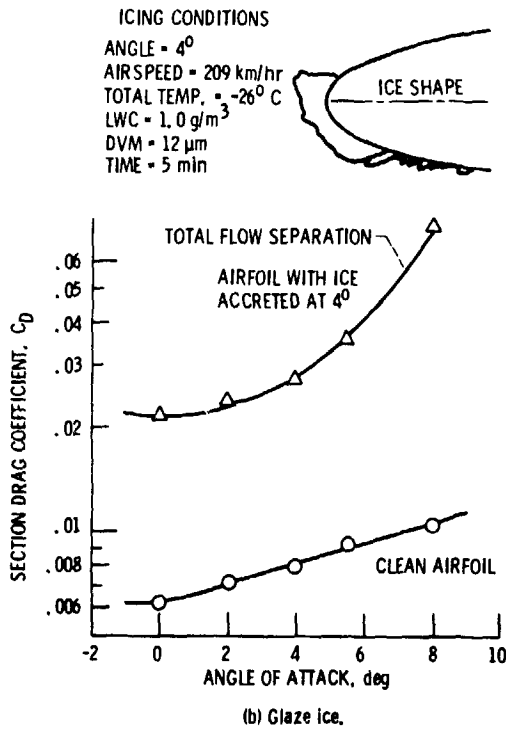
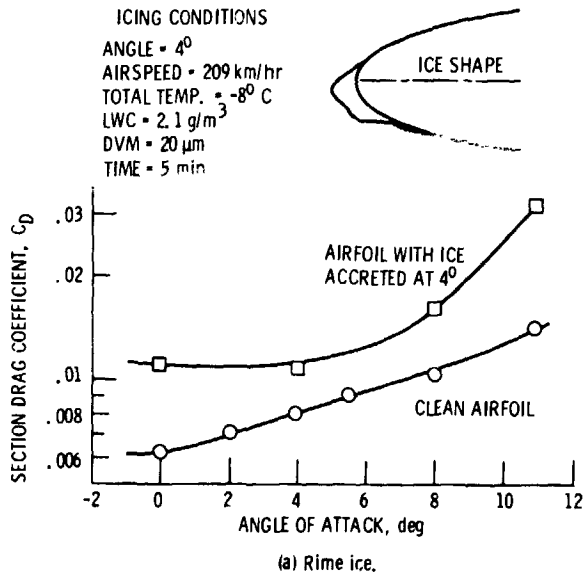
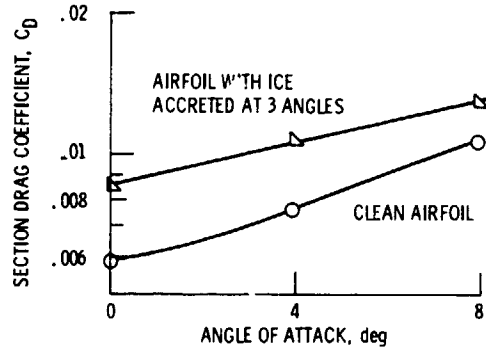
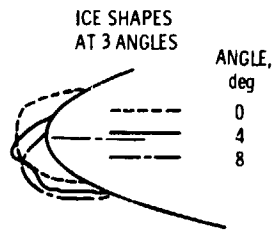


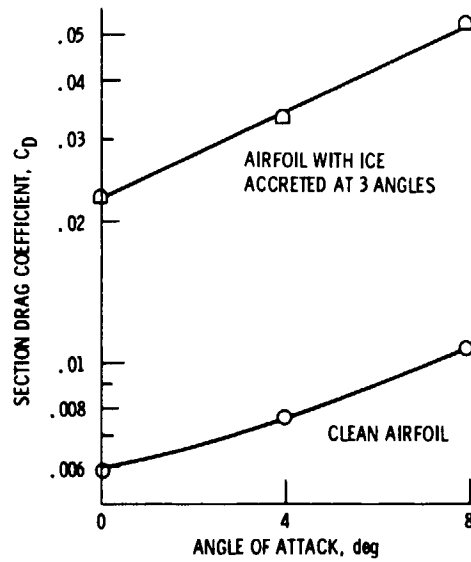
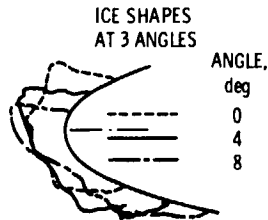
Figure 6. - Variation of the drag coefficient with angle of attack for ice accreted at a 4° angle of attack.

ICING CONDITIONS
 TOTAL TEMP. = -26°C
 AIRSPEED = 209 km/hr
 LWC = 1.0 g/m^3
 DVM = $12\text{ }\mu\text{m}$
 TIME = 5 min



(a) Rime ice,

ICING CONDITIONS
 TOTAL TEMP. = -8°C
 AIRSPEED = 209 km/hr
 LWC = 2.1 g/m^3
 DVM = $2\text{ }\mu\text{m}$
 TIME = 5 min



(b) Glaze ice,

Figure 7. - Ice shape and drag for ice accreted at 3 angles.

CASE	AIR SPEED, km/hr	TEMP., °C	LWC g/m ³	DWV µm
A, B, C	209	-8	2.1	20
D, E, F	209	-26	1.0	12

21 INCH CHORD 0012 AIRFOIL

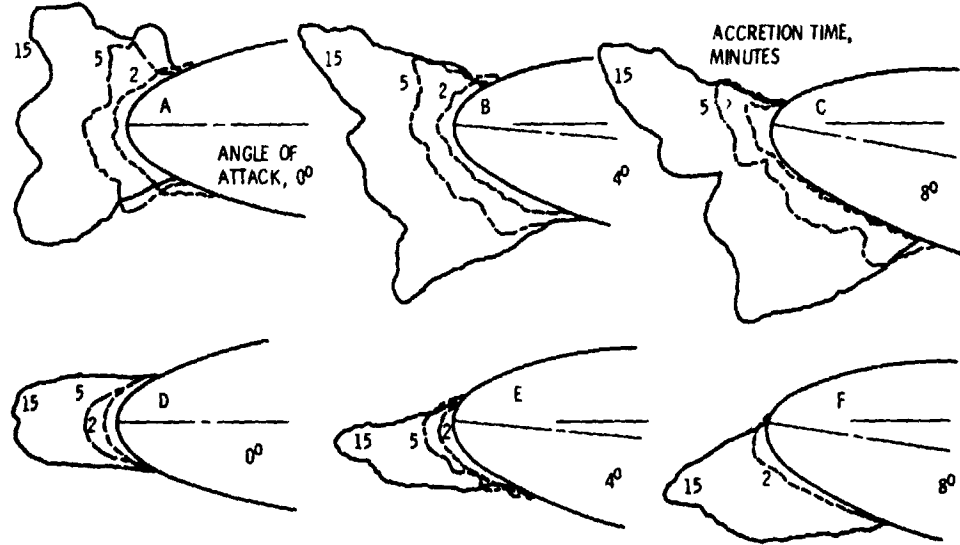
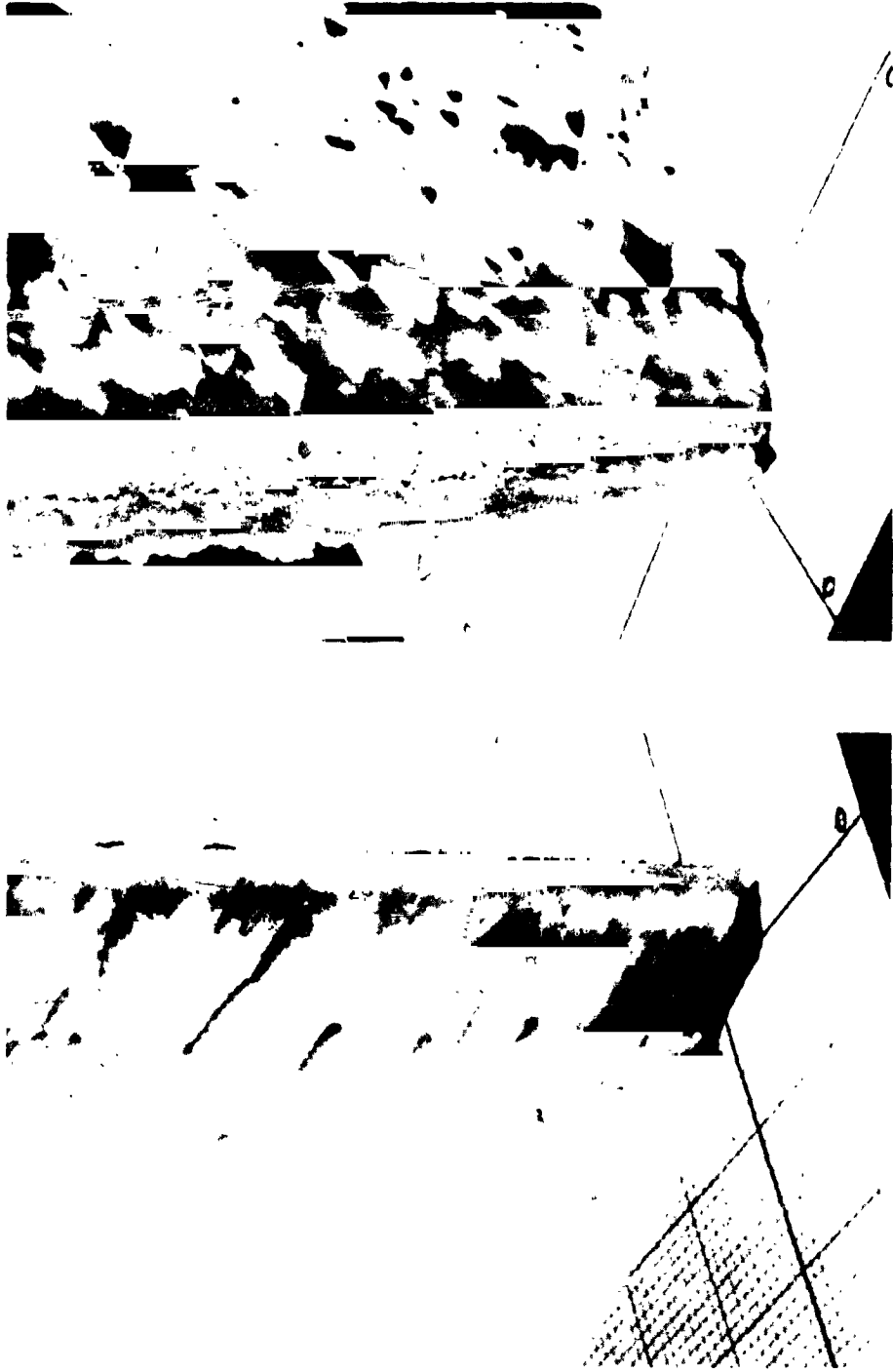


Figure 8. - Effect of time and the angle of attack on the ice shape airfoil, NACA 0012 with a 0.53-m-chord.

ORIGINAL COPY
OF POOR QUALITY



(a) Suction side.

(b) Pressure side.

Figure 9. - Photographs of the ice accretion at -18°C . Airspeed, 209 km/hr ; LWC, 1.3 g/m^3 ; DVM, $20\mu\text{m}$; Time, 8 min.; Airfoil, 0.53 m chord 0012 airfoil at 4 deg. angle.

OF ICE

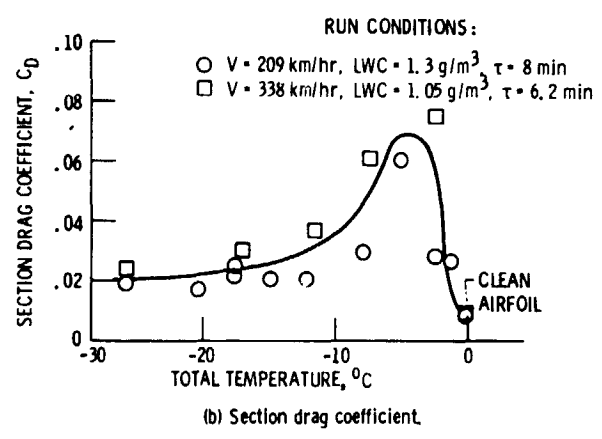
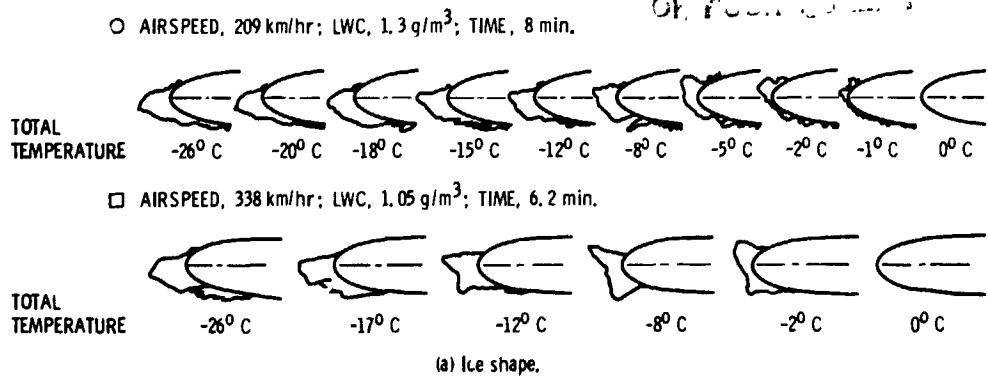


Figure 10. - Effect of total temperature on the ice shape and drag. (LWC x V x time) = const.; DVM, 20 μm; .053-m-chord 0012 airfoil at a 4° angle of attack.

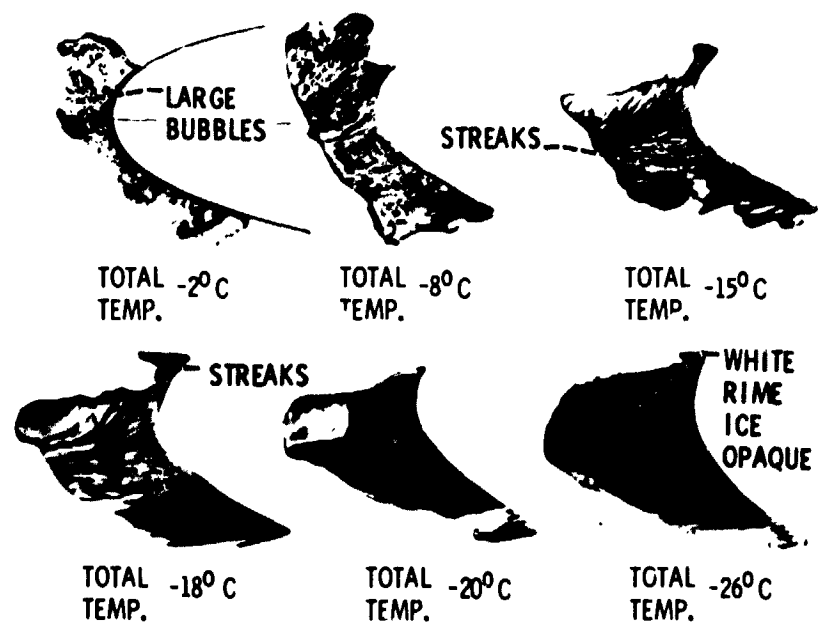


Figure 11. - Effect of temperature on the ice structure. Thin ice samples removed from the airfoil and backlighted; Airspeed, 209 km/hr; LWC, 1.3 g/m³; DVM, 20 μm; Time, 8 min; Airfoil, 0.53 m chord 0012 airfoil at 4 deg. angle.

ORIGINAL PHOTOGRAPH
OF POOR QUALITY



GLAZE ICE
(large crystals)

RIME ICE
(small crystals)

Figure 12. - Ice crystal size using polarized light.

C-82-6712

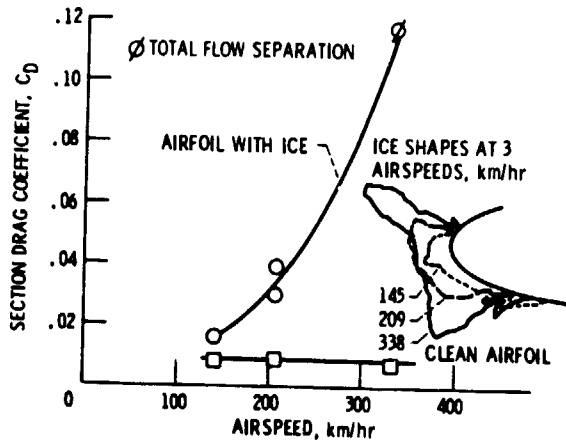
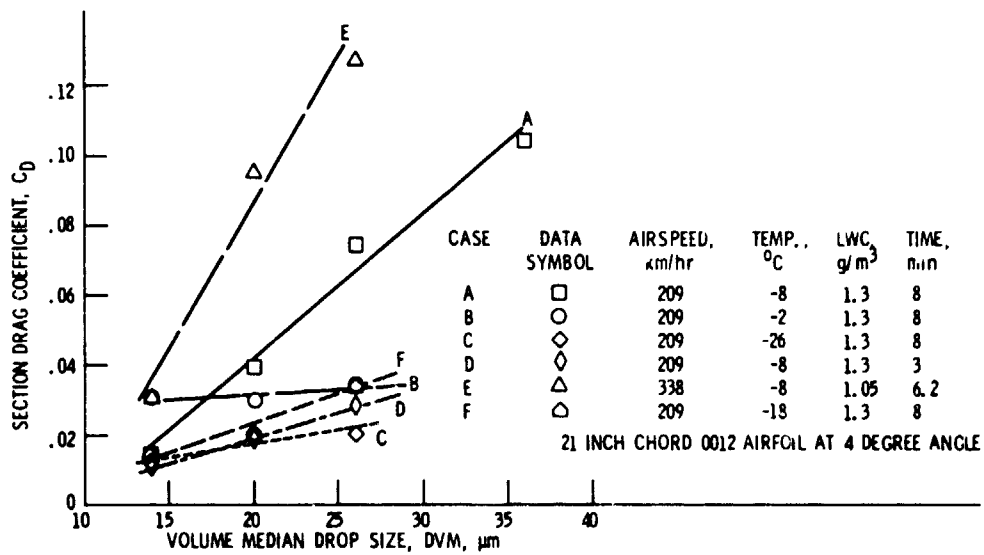
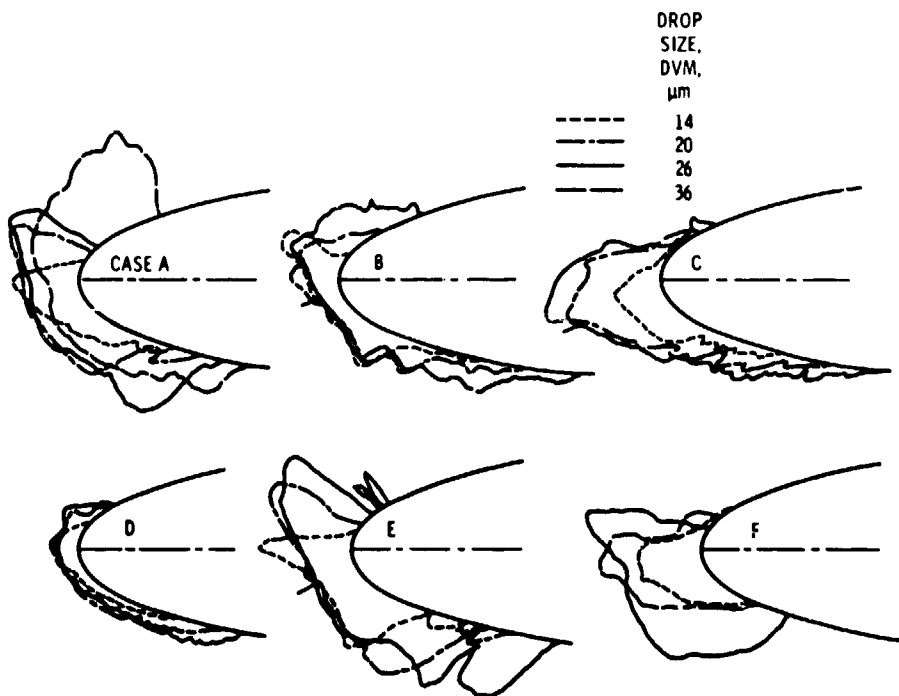


Figure 13. - Effect of velocity on the ice shape and section drag. Total temperature, -8°C ; LWC, 1.3 g/m^3 ; DVM, $20\text{ }\mu\text{m}$; time, 8 min; airfoil, .53-m-chord 0012 airfoil at 4° angle of attack.



(a) Drag coefficient.



(b) Ice shape.

Figure 14. - Effect of droplet size on shape and drag. Airfoil, .053-m-chord 0012 airfoil at 4° angle.

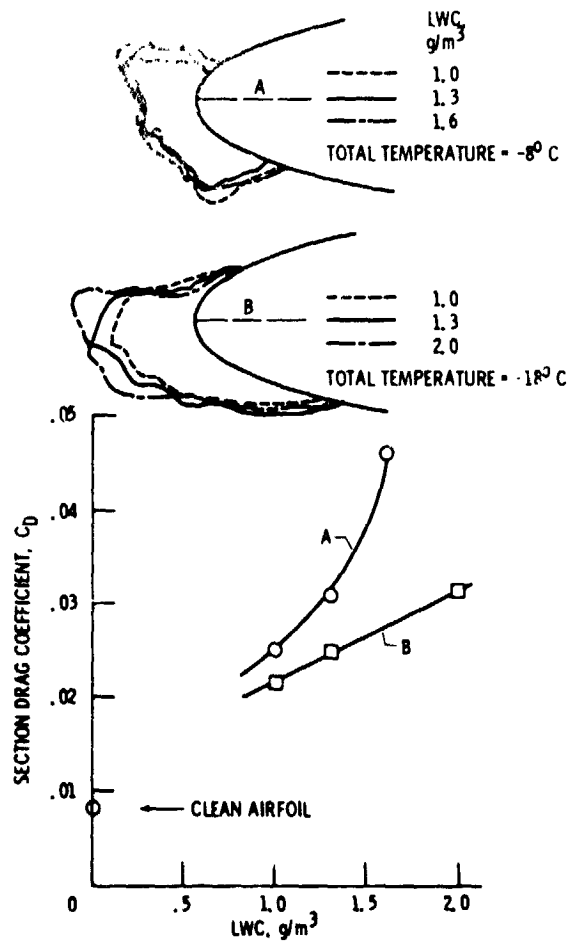


Figure 15. - Effect of LWC on the ice shape and section drag. Airspeed, 209 km/hr; DVM, 20 μm ; time, 8 min; airfoil, .53-m-chord 0012 airfoil at 4° angle of attack.

CLAY
OF ICE

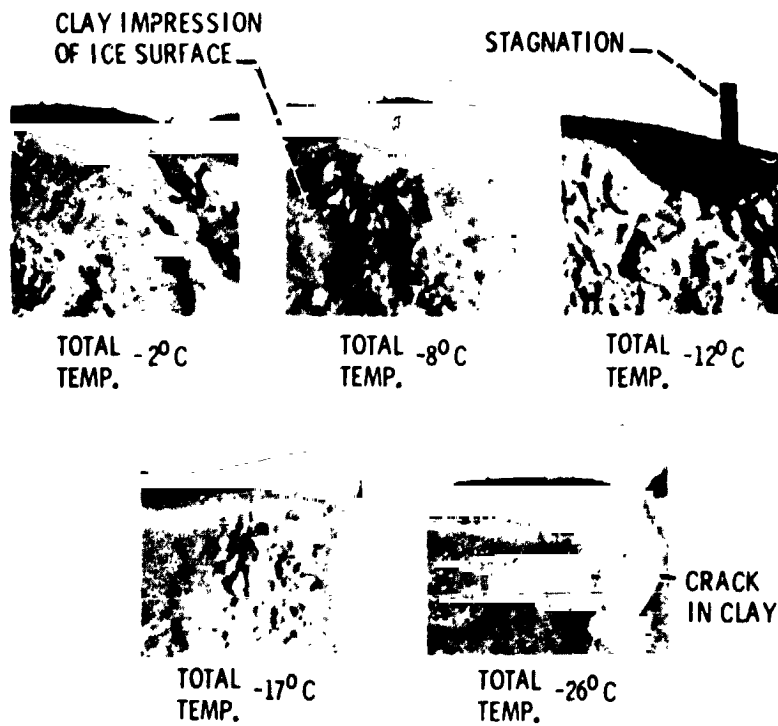


Figure 16. - Effect of temperature on the roughness of the ice surface in stagnation region; Airspeed, 338 km/hr; DVM, 20 μ m; LWC, 1.05 g/m³; Time, 6.2 min.; Airfoil, .053 m chord 0012 airfoil at 4 deg. angle.

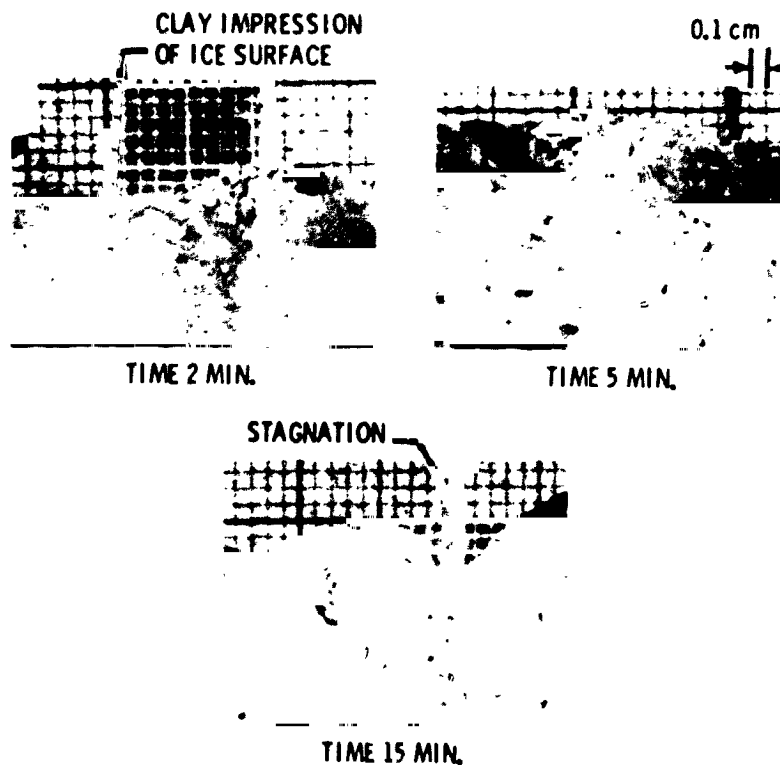


Figure 17. - Effect of time on the roughness of the ice surface in stagnation region. Airspeed, 209 km/hr; Total temp., -8C; DVM, 20 μ m; LWC, 2.1 g/m³; Airfoil, .53 m chord 0012 airfoil at 4 deg. angle of attack.

ORIGINAL
OF POOR QUALITY

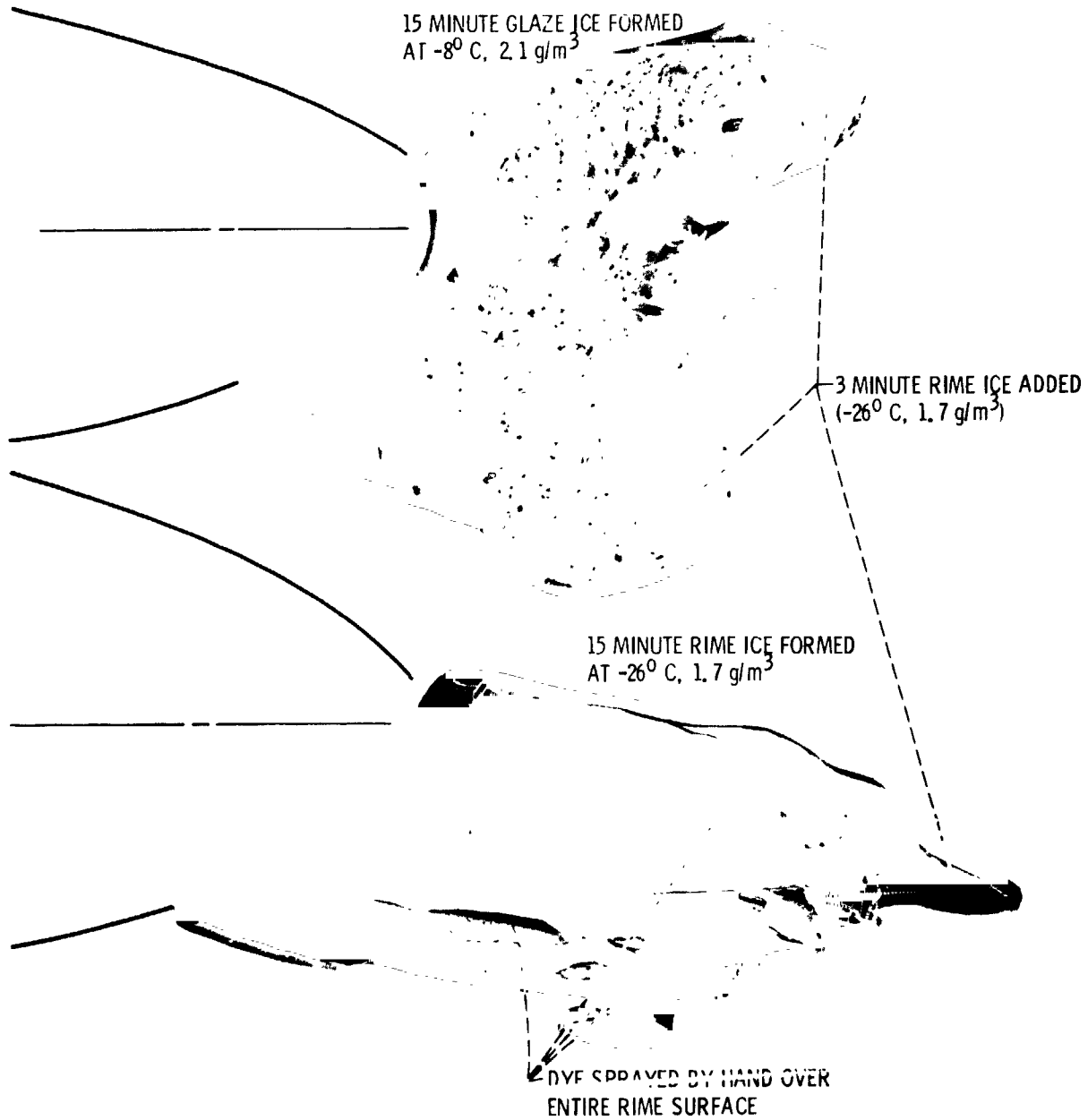


Figure 18. - The effect of the ice shape on the droplet catch. Backlighted thin ice sample of a 3 minute rime spray on top of the initial ice shape. For all sprays: DVM, $20\mu\text{m}$; airspeed, 209 km/hr.

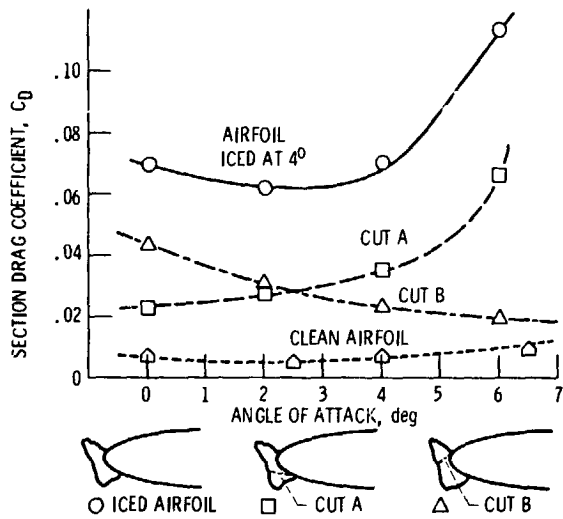


Figure 19. - Effect of partial ice removal on the drag.
 Conditions for the initial ice: total temperature, -8°C ;
 airspeed, 338 km/hr; DVM, $20\ \mu\text{m}$; LWC, 1.05 g/m;
 airfoil, .053-m-chord 0012 airfoil at 4° .

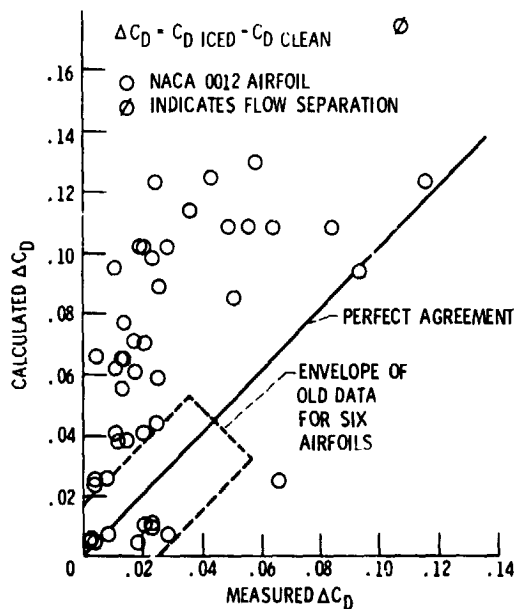


Figure 20. - Comparison of measured drag coefficient with values predicted by old correlation (ref. 1) for 0012 airfoil over a wide range of icing conditions.

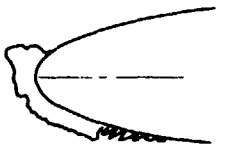
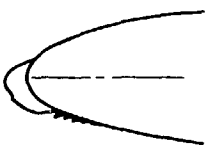
ICE SHAPE (FROST REMOVED)				
ICING CONDITIONS: AIRSPEED TEMPERATURE ANGLE OF ATTACK LWC DVM TIME	209 km/hr -8° C 4° 2.1 g/m ³ 20 μm 5 min	209 km/hr -26° C 4° 1.0 g/m ³ 12 μm 5 min		
DRAG COEFFICIENT AS ICE SPAN IS REDUCED:	C_D	AMOUNT OF CHANGE IN C_D , PERCENT	C_D	AMOUNT OF CHANGE IN C_D , PERCENT
(a) CEILING TO FLOOR (1.8 m) (b) MIDDLE 1.2 m (c) MIDDLE 0.6 m (d) MIDDLE 0.3 m	0.0338 .0351 .0345 .0326	0 (REF.) 3.5 2.0 -3.6	0.0100 ----- .0098 .0093	0 (REF.) ----- -2.3 -7.7

Figure 21. - Effect of reducing the span of the ice on the measured section drag coefficient.

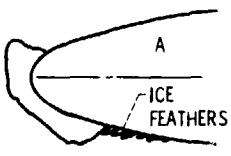
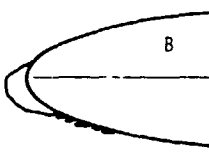
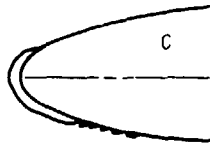
ICE SHAPE						
CONDITIONS: AIRSPEED TEMPERATURE ANGLE OF ATTACK LWC DVM TIME	209 km/hr -8° C 4° 2.1 g/m ³ 20 μm 5 min	209 km/hr -26° C 4° 1.05 g/m ³ 12 μm 5 min	209 km/hr -26° C 4° 1.05 g/m ³ 20 μm 5 min			
DRAG COEFFICIENT FOR:	C_D	AMOUNT OF CHANGE IN C_D , PERCENT	C_D	AMOUNT OF CHANGE IN C_D , PERCENT	C_D	AMOUNT OF CHANGE IN C_D , PERCENT
(a) AS SPRAYED (b) FROST REMOVED (c) LOWER SURFACE ICE FEATHERS REMOVED	0.0398 .0373 .035	6.7 0 (REF.) -6.1	0.0167 .0105 .0087	59.0 0 (REF.) -17.6	0.0122 .0107 .0102	14.0 0 (REF.) -5.2

Figure 22. - Effect of frost and lower surface ice feathers on the measured section drag coefficient of the NACA0012 airfoil, $c = 0.533$ m. (From ref. 18.)

1. Report No. NASA TM-83556	2. Government Accession No.	3. Recipient's Catalog No.	
4. Title and Subtitle Ice Shapes and the Resulting Drag Increase for a NACA 0012 Airfoil		5. Report Date	
		6. Performing Organization Code 505-45-12	
7. Author(s) William Olsen, Robert Shaw, and James Newton		8. Performing Organization Report No. E-1935	
		10. Work Unit No.	
9. Performing Organization Name and Address National Aeronautics and Space Administration Lewis Research Center Cleveland, Ohio 44135		11. Contract or Grant No.	
		13. Type of Report and Period Covered Technical Memorandum	
12. Sponsoring Agency Name and Address National Aeronautics and Space Administration Washington, D.C. 20546		14. Sponsoring Agency Code	
		15. Supplementary Notes Prepared for the Twenty-second Aerospace Sciences Meeting sponsored by the American Institute of Aeronautics and Astronautics, Reno, Nevada, January 9-12, 1984.	
16. Abstract Experimental measurements of the ice shapes and resulting drag increases were measured in the NASA-Lewis Icing Research Tunnel. The measurements were made over a large range of conditions (e.g., airspeed and temperature, drop size and liquid water content of the cloud, and the angle of attack of the airfoil). The measured drag increase did not agree with the existing correlation. Additional results were given which are helpful in understanding the ice structure and the way it forms, and in improving the ice accretion modeling theories. There are data on the ice surface roughness, on the effect of the ice shape on the local droplet catch, and on the relative importance of various parts of the ice shape on the drag increase. Experimental repeatability is also discussed.			
17. Key Words (Suggested by Author(s)) Icing Rotor blade		18. Distribution Statement Unclassified - unlimited STAR Category 03	
19. Security Classif. (of this report) Unclassified	20. Security Classif. (of this page) Unclassified	21. No. of pages	22. Price*